J. Fluid Mech. (1998), *vol.* 371, *pp.* 301–318. Printed in the United Kingdom

© 1998 Cambridge University Press

Two-layer flow past a cylinder in a rotating frame

By PETER BLANCHONETTE†

Centre for Dynamical Meteorology and Oceanography, Monash University, Clayton, Victoria 3168, Australia

(Received 14 November 1996 and in revised form 5 May 1998)

In this paper the two-layer flow past a cylinder in a rotating frame is modelled numerically. This study follows on from the many theoretical and experimental examinations of the one-layer flow past a cylinder. The main aim of this study is to investigate the geophysically relevant effect on the flow of varying the vertical shear, while keeping the other parameters the same in both layers. This will include an examination of the contour plots of vorticity and streamfunction and measuring the size of the separated region and the position of separation as a function of the vertical shear. The most interesting result is that the separated region in the slower layer grows much larger than that in the faster layer as the vertical shear is increased.

1. Introduction

The background rotation of the Earth plays an important role in many geophysical flows, such as the flow past an island (Etling 1990). In Blanchonette (1997*a*) the effects of background rotation on the flow past a cylinder were examined for both steady and unsteady flows. The flow patterns observed were found to vary, sometimes markedly, from those found in the non-rotating-frame case, due to the efficient dissipation of vorticity via Ekman friction. Specifically, flow separation and unsteadiness can develop for much larger Reynolds numbers than observed in the non-rotating flow. Also, an asymmetry was observed in the wake of the cylinder, in contrast to the symmetric wake in the non-rotating flow.

The stratification of the atmosphere and oceans can also play an important role in many geophysical flows, such as the flow past a mountain range (Baines 1979) or a seamount (Thompson 1993). To gain a greater understanding of geophysical flows in which both stratification and rotation are important the effect of stratification on the flow past a cylinder in a rotating frame is examined. To do this in the simplest way possible a two-layer model was chosen; each layer of fluid being homogeneous, the stratification was concentrated at the interface. The main aim of this paper is to investigate the effect on the steady flow of varying the vertical shear while keeping the other non-dimensional parameters the same in both layers. The most surprising result to be revealed by this study is the rapid growth of the separated region in the slower layer of fluid as the vertical shear increases.

1.1. *The two-layer approximation*

Quite distinct layers of fluid occur in nature, and some examples of these include when a layer of warm water lies above cold water or fresh water above salt water; an abrupt

† Present address: Air Operations Division, AMRL, PO Box 4331, Melbourne Vic. 3001, Australia, email: Peter.Blanchonette@dsto.defence.gov.au.

https://doi.org/10.1017/S0022112098002262 Published online by Cambridge University Press

change also occurs between the atmosphere and ocean. Continuously stratified flows can often be modelled to a first approximation using multi-layer models. In these models each layer is of constant density with the stratification concentrated at the interface. Two-layer models have been used for a wide range of problems, for example, baroclinic instability, the formation of bottom water and the flow past topography.

1.1.1. *The two-layer flow past a cylinder in a rotating frame*

A two-layer model has also been used to examine the effect of stratification on the flow past a cylinder in a rotating frame. Brevdo & Merkine (1985) considered this problem for the f-plane case, where the main aim was to examine the effect of vertical shear on the flow. A further analysis of this study will appear in Blanchonette & Page (1998). Firstly, Brevdo & Merkine studied the linear Stewartson layer and demonstrated that when the vertical shear is sufficiently strong the wall velocity and shear stress in the slower layer are of opposite sign to those in the faster layer. Following this, Brevdo & Merkine explored the nonlinear form of the $E^{1/4}$ layer, which involved using a boundary-layer numerical model to examine the radial velocity profiles and shear stress on the surface of the cylinder. The velocity profiles and shear-stress curves were examined for three different combinations of advection strength and vertical shear and they found that it was possible to have flow reversal in the slower layer without the flow separating when the vertical shear was strong. They also studied the variation of the point of separation and flow reversal when the vertical shear is strong, with the point of separation taken to be where the numerical model ceased to converge. They found that, initially, flow reversal commenced close to the rear stagnation point and separation near the front stagnation point. As the strength of the advection increased the two points slowly merged at approximately 100° from the front of the cylinder.

A criterion was also derived for the flow in the upper and lower layers to remain attached. As the flow approached separation it began to behave as a single-layer fluid (which they referred to as barotropization), which lead them to suggest that the criterion in the upper layer could be used as a criterion for fully attached flows in both layers.

Merkine & Brevdo (1986) included the effect of the β-plane in their boundary-layer model. Two parameter régimes were examined, namely $0 \leqslant E^{1/2}/Ro \leqslant \infty$, $\beta = O(1)$ and $E^{1/2}/Ro \gg 1$, $\beta Ro/E^{1/2} = O(1)$. For the first parameter range they found 'the enhancement/suppression of separation in the retrograde/prograde flows and the east-west asymmetry observed in the experiments of Boyer & Davies (1982)'. In the second parameter range they examined they found that when the oncoming flow was vertically sheared large eddies could be formed at the rear of the cylinder.

The configuration of the two-layer flow past a cylinder in a rotating frame will now be explained and the non-dimensionalized equations which describe the flow derived.

2. Governing equations

Consider the uniform flow of two layers of homogeneous, immiscible fluid of depth d_1^* and d_2^*, densities ρ_1^* and ρ_2^* and corresponding kinematic viscosities ν_1^* and ν_2^* past a right circular cylinder of radius l^*. The density of the fluid in the top layer (layer one) is slightly less than that in the bottom layer (layer two), so the system is gravitationally stable and the Boussinesq approximation is valid. The cylinder is aligned with the vertical axis and is placed between two parallel plates of infinite extent a distance d^* apart. The whole system rotates in an anti-clockwise direction

https://doi.org/10.1017/S0022112098002262 Published online by Cambridge University Press

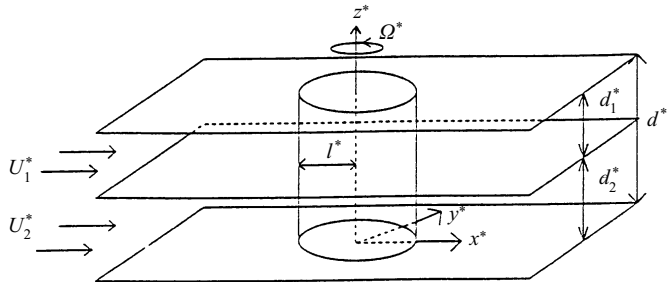


FIGURE 1. The geometrical configuration of the two-layer flow past a cylinder.

about an axis parallel to the z^*-axis with angular velocity Ω^*. The two layers have free-stream speeds U_1^* and U_2^*, relative to the rotating frame. The centrifugal forces are assumed to be negligible, so when there is no motion the interface remains level. The configuration of this problem is shown in figure 1.

The equations which govern the flow can be non-dimensionalized with

$$\boldsymbol{u}_i = \frac{\boldsymbol{u}_i^*}{U^*}, \quad \boldsymbol{x}_i = \frac{\boldsymbol{x}_i^*}{l^*}, \quad d_i = \frac{d_i^*}{l^*} \quad \text{and} \quad t = T\Omega^* t^*, \tag{2.1}$$

where $\boldsymbol{x}_i = (x_i, y_i, z_i)$ are Cartesian coordinates in layer i measured relative to the rotating frame, $\boldsymbol{u}_i = (u_i, v_i, w_i)$ is the flow velocity in layer i measured relative to the rotating frame, d_i is the depth of layer i (assumed to be of order unity) and T is a characteristic timescale of the motion (which is undefined at this time).

Following this scaling, the governing equations in each layer become

$$T\frac{\partial \boldsymbol{u}_i}{\partial t} + Ro\,(\boldsymbol{u}_i \cdot \nabla)\,\boldsymbol{u}_i + 2\,(\boldsymbol{k} \times \boldsymbol{u}_i) = -\nabla P_i + d_i^2 E_i \nabla^2 \boldsymbol{u}_i \tag{2.2}$$

and

$$\nabla \cdot \boldsymbol{u}_i = 0, \tag{2.3}$$

where the reduced pressure P_i has been scaled by $\rho_i^* U_i^* \Omega^* l^*$. As in the one-layer case, the Rossby and Ekman numbers can be defined as $Ro = U^*/\Omega^* l^*$ and $E_i = \nu_i^*/\Omega^* d_i^{*2}$, respectively, where $U^* = \frac{1}{2}(U_1^* + U_2^*)$ is a characteristic horizontal velocity of the flow. Considering the case of steady flow with $Ro \ll 1$ and $E_i \ll 1$ the leading-order equation (2.2) in both layers is $2\,(\boldsymbol{k} \times \boldsymbol{u}_i) = -\nabla P_i$, which implies that the flow is geostrophic and depth independent to leading order in each layer (Greenspan 1968). Thus, a streamfunction can be defined in both layers of the form $u_i = -\partial\psi_i/\partial y$ and $v_i = \partial\psi_i/\partial x$.

It can be shown that the vertical component of the vorticity $\zeta_i = (\nabla \times \boldsymbol{u}_i) \cdot \boldsymbol{k}$ satisfies

$$T\frac{\partial \zeta_i}{\partial t} + Ro(\boldsymbol{u}_i \cdot \nabla_h)\zeta_i = (2 + Ro\zeta_i)\frac{\partial w_i}{\partial z} + d_i^2 E_i \nabla_h^2 \zeta_i, \tag{2.4}$$

where $\nabla_h = (\partial/\partial x, \partial/\partial y, 0)$ is the horizontal gradient term in Cartesian coordinates and $\nabla_h^2 = \partial^2/\partial x^2 + \partial^2/\partial y^2$ is the horizontal Laplacian in Cartesian coordinates. The term $\partial w_i/\partial z$ is included so that the effect of the vortex stretching, caused by the Ekman layers on the top and bottom plates and the interface, can be examined. From the definition of the vertical vorticity $\zeta_i = (\nabla \times \boldsymbol{u}_i) \cdot \boldsymbol{k}$ it follows that $\nabla_h^2 \psi_i = \zeta_i$, which is known as the Poisson equation.

In the problem examined here the interface does not move to leading order, although the vertical velocity of the interface is included so that the effect of the sloping of

https://doi.org/10.1017/S0022112098002262 Published online by Cambridge University Press

the interface can be examined. The height of the interface is $z = d_2 + \frac{1}{2}RoF\eta$, where $\eta = \psi_2 - \psi_1$ and $F = f_0^{*2}l^*/(g^*\Delta\rho^*/\rho_2^*)$. Applying the Ekman compatibility conditions at $z = 0, d$ including the vertical velocity of the interface gives (outside of the Ekman layers) in the top layer

$$\frac{\partial w_1}{\partial z} = -\frac{1}{2}E_1^{1/2}\zeta_1 - \frac{F_1}{2}\frac{\mathrm{D}\eta}{\mathrm{D}t} - \frac{1}{2}E_1^{1/2}\frac{\chi}{\chi+1}(\zeta_1 - \zeta_2) \tag{2.5}$$

and in the bottom layer

$$\frac{\partial w_2}{\partial z} = -\frac{1}{2}E_2^{1/2}\zeta_2 + \frac{F_2}{2}\frac{\mathrm{D}\eta}{\mathrm{D}t} - \frac{1}{2}E_2^{1/2}\frac{\chi}{\chi+1}(\zeta_2 - \zeta_1), \tag{2.6}$$

where $F_i = f_0^{*2}l^{*2}/g^*d_i^*(\Delta\rho^*/\rho_2^*)$ and the $O(RoF\eta)$ variations were neglected when calculating the z derivatives.

In this study all the non-dimensional parameters are kept the same in both layers, except for the free-stream speed (hence $E_i = E$, $F_i = F$ and $d_i = d$) so the effect of varying the strength of the vertical shear can be examined. For $Ro = O(E^{1/2})$ and letting $T = 2E^{1/2}$, which is the timescale of the Ekman friction, the governing equations are

$$\frac{\partial\zeta_1}{\partial t} + \lambda(\boldsymbol{u}_1\cdot\nabla_h)\zeta_1 = (1+\tfrac{1}{2}Ro\zeta_1)\left[\frac{1}{2}\left(-\zeta_1 + \frac{\chi}{1+\chi}(\zeta_2-\zeta_1)\right) - F\frac{\mathrm{D}\eta}{\mathrm{D}t}\right] + \delta^2\nabla_h^2\zeta_1 \tag{2.7}$$

and

$$\frac{\partial\zeta_2}{\partial t} + \lambda(\boldsymbol{u}_2\cdot\nabla_h)\zeta_2 = (1+\tfrac{1}{2}Ro\zeta_2)\left[\frac{1}{2}\left(-\zeta_2 + \frac{1}{1+\chi}(\zeta_1-\zeta_2)\right) + F\frac{\mathrm{D}\eta}{\mathrm{D}t}\right] + \delta^2\nabla_h^2\zeta_2, \tag{2.8}$$

where $\lambda = Ro/2E^{1/2} = O(1)$ and $\delta = d\left(\frac{1}{2}E^{1/2}\right)^{1/2} \ll 1$, where δ is the scaled-boundary-layer thickness. Writing $\Gamma_1 = \zeta_1 + F\eta$ and $\Gamma_2 = \zeta_2 - F\eta$ equations (2.7) and (2.8) become

$$\frac{\partial\Gamma_1}{\partial t} + \lambda(\boldsymbol{u}_1\cdot\nabla_h)\Gamma_1 = \frac{1}{2}\left[-\zeta_1 + \frac{\chi}{\chi+1}(\zeta_2-\zeta_1)\right] + \delta^2\nabla_h^2\zeta_1 \tag{2.9}$$

and

$$\frac{\partial\Gamma_2}{\partial t} + \lambda(\boldsymbol{u}_2\cdot\nabla_h)\Gamma_2 = \frac{1}{2}\left[-\zeta_2 + \frac{\chi}{\chi+1}(\zeta_1-\zeta_2)\right] + \delta^2\nabla_h^2\zeta_2, \tag{2.10}$$

respectively, where Γ_i is the potential vorticity in layer i. As a result of defining a characteristic velocity U^* it is required that $U_1 + U_2 = 2$. In this study the effects of the sloping of the interface are to be examined, so $F = O(1)$. Subtracting the Poisson equation in layer two from the Poisson equation in layer one gives the Helmholtz equation

$$\nabla^2(\psi_2 - \psi_1) - 2F(\psi_2 - \psi_1) = \Gamma_2 - \Gamma_1, \tag{2.11}$$

which is used so that $\psi_2 - \psi_1$ can be found given Γ_i, and hence ψ_1 and ψ_2 individually.

The boundary conditions that apply to this flow are that the streamfunction in each layer matches onto the appropriate uniform flow at infinity, so that $\psi_i \sim -U_i y$ and $\zeta_i = 0$ as $r \to \infty$, and that both ψ_i and $\partial\psi_i/\partial r$ are zero on $r = 1$.

The numerical method used to solve the governing equations is essentially the same as used in the one-layer case; this is described in detail in Blanchonette (1995). Briefly, the physical domain is conformally transformed to the computational domain using the same transformation that was employed in the one-layer case. The governing

https://doi.org/10.1017/S0022112098002262 Published online by Cambridge University Press

equations are solved on the same stretched grid in each layer; the stretching used in both directions was the same as that used in the one-layer method and typically a 128 by 128 grid was used. In the current study the scaled-boundary-layer thickness was the same in both layers; this meant the grid used in both layers could be the same without affecting the resolution in the $E^{1/4}$ layer.

The solution process begins by calculating the initial values of the vorticity and streamfunction in both layers using the method outlined in the Blanchonette (1995). In order to solve the potential vorticity equations (2.9), (2.10) in both layers the alternating-directions-implicit method was used. The Helmholtz equation and the Poisson equation were inverted using the multigrid package mgd9v (de Zeeuw 1990). The no-slip boundary condition on the surface of the cylinder was implemented in a similar fashion to Becker (1989), which in turn was based upon a modified form of that in Israeli (1972).

3. Results

3.1. *Introduction*

The numerical method described previously was used to solve the governing equations in both layers over a wide range of the non-dimensional parameters. In this paper the main focus will be on exploring the effect of variation of the vertical shear on the steady symmetric flows, while keeping the other parameters (namely λ, δ and F) the same in both layers. This will include examining the variation of the separation point and size of the separated regions with increasing vertical shear. The most interesting result is the rapid growth of the separated region in the slower layer as the vertical shear is increased. In §3.2 contour plots of the vorticity and streamfunction will be presented and in these cases $F = 1$ in both layers and $\chi = 1$.

3.2. *Parameter study*

In this subsection the effects of increasing the strength of the advection and viscous diffusion will be examined, by increasing λ and δ (the scaled-boundary-layer thickness), respectively. In the first series of contour plots, depicted in figure 2, $\lambda = 0$ and $\delta = 0.1$. For $\lambda = 0$ the vorticity equation is linear and there is no advection of the flow. If both U_1 and U_2 are 1 then the two layers are identical and the contour plots are the same as the one-layer case with a scaled-boundary-layer thickness of 0.14 (since the scaled depth is twice that of the two-layer case). When $U_1 = 1.2$ (U_1 is the free-stream speed in the upper layer), and hence $U_2 = 0.8$, the vorticity contours in the upper and lower layers appear similar. Note that no vorticity is advected downstream, so that the only mechanism for the spread of vorticity is through lateral diffusion and through the interaction between the two layers. The streamfunction contour plots show that the flow in both layers is symmetric across the y-axis, resembling potential flow, except close to the cylinder.

Increasing U_1 to 1.5 (not shown) results in contour plots of the vorticity and streamfunction that appear similar to the plots for $U_1 = 1.2$, but they are slightly different close to the cylinder due to the interaction between the layers. Increasing the vertical shear further, so that $U_1 = 1.8$ (figure 2*b*), the plots of the vorticity and streamfunction in the upper layer appear similar to the one-layer flow. In the lower layer the streamfunction plot shows that the zero streamline has separated from the cylinder and hence the flow is reversed right around the cylinder. Thus, positive vorticity is generated on the top (meaning the left side of the cylinder looking downstream) of the cylinder and negative vorticity on the bottom (meaning the right

https://doi.org/10.1017/S0022112098002262 Published online by Cambridge University Press

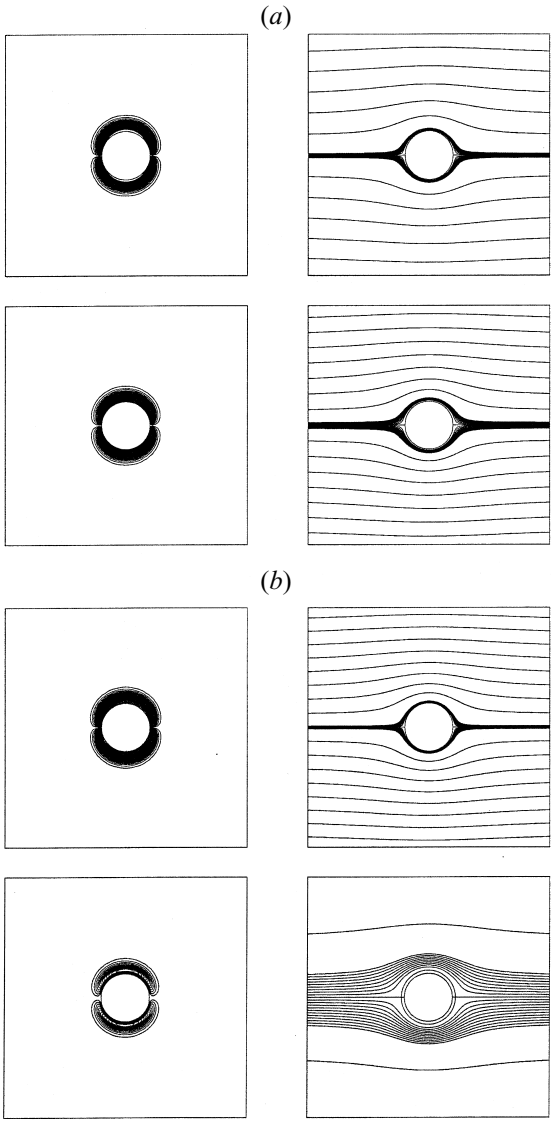


FIGURE 2 (*a–b*). For caption see facing page.

side of the cylinder looking downstream) of the cylinder in this layer. Above the top of the cylinder there are negative contours of vorticity while below the cylinder positive contours are present. This vorticity comes from the interaction between the two layers through the Ekman layers that form at the interface, which was originally noted by Brevdo & Merkine (1985).

If U_1 is increased to 2.0 (figure 2*c*), so that the flow speed at infinity in the lower layer is zero, the vorticity contours in the upper layer show little change from the previous cases, with the streamlines resembling potential flow. In the lower layer some of the vorticity is detached from the cylinder, as in the previous case. The streamfunction contours in the lower layer have a dipole-like structure, with the flow reversed around the whole cylinder.

https://doi.org/10.1017/S0022112098002262 Published online by Cambridge University Press

(*c*)

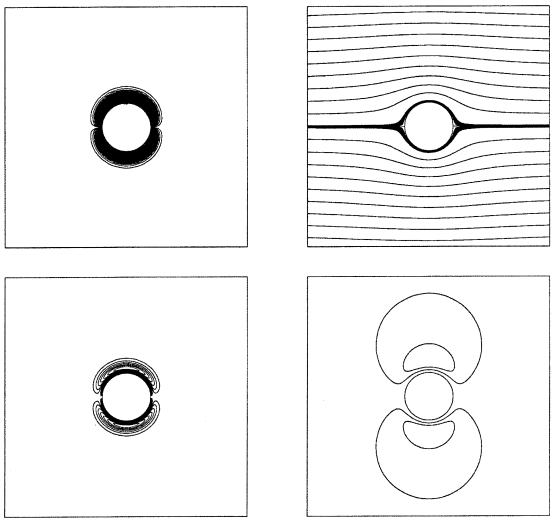


FIGURE 2. Contour plots of vorticity (left) and streamfunction (right) for $\lambda = 0$, $\delta = 0.1$, $F = 1$, $\chi = 1$ and (*a*) $U_1 = 1.2$, (*b*) $U_1 = 1.8$ and (*c*) $U_1 = 2.0$. The top plots are for the upper layer and the bottom plots are for the lower layer. The contour interval for the vorticity is 0.1 in both layers. The streamfunction contour interval is 1.0 in the upper layer, except close to the cylinder where it is 0.01. In the lower layer the streamfunction contour interval is 0.5, except close to the cylinder where it is 0.01. When $U_1 \geqslant 1.8$ the contour interval of the streamfunction is 0.02 close to the cylinder in the lower layer.

In the second series of contour plots, shown in figure 3, λ is increased to 2, but with the same value of δ as in figure 2. Again, the vertical shear is varied to examine the effect of variation of this parameter. In figure 3(*a*), where $U_1 = 1.2$ and $U_2 = 0.8$, the contour plots of the vorticity appear quite similar in both layers, except that the vorticity in the upper layer is advected slightly further downstream than in the lower layer. This is to be expected since the free-stream speed is larger in the upper layer than in the lower layer. The contour plots of the streamfunction show that the flow has separated from the surface of the cylinder in both layers. The upper-layer separation bubble is slightly larger (as measured by the position of reattachment of the zero streamline), being about one cylinder radius in length. This is consistent with the effect of advection in the one-layer flow, where the separation bubble is larger in the faster flows (note that the effective values of λ in both layers are really λU_1 and λU_2, respectively). Also, the flow inside the upper- and lower-layer bubbles is almost stagnant. As Matsuura & Yamagata (1985) noted for the one-layer flow, this is due to the spin-down of the standing eddies at the rear of the cylinder (a more detailed explanation of the effect of the Ekman layers is given in Blanchonette 1995).

Increasing the vertical shear further, figure 3(*b*) shows the case of $U_1 = 1.5$ and $U_2 = 0.5$. Comparing the vorticity contour plots for each layer, it appears that the vorticity is advected further downstream in the upper layer than in the lower layer, as may be expected, since the free-stream speed is three-times larger in the upper layer. Studying the contour plots of the streamfunction it can be seen, rather surprisingly, that the size of the separation bubble in the lower layer is larger than that in the upper layer. It can also be seen by the streamline density in the lower layer that the flow in the lower-layer separation bubble is faster than that in the upper-layer bubble, although the flow is still quite slow relative to the flow outside the shear layer.

https://doi.org/10.1017/S0022112098002262 Published online by Cambridge University Press

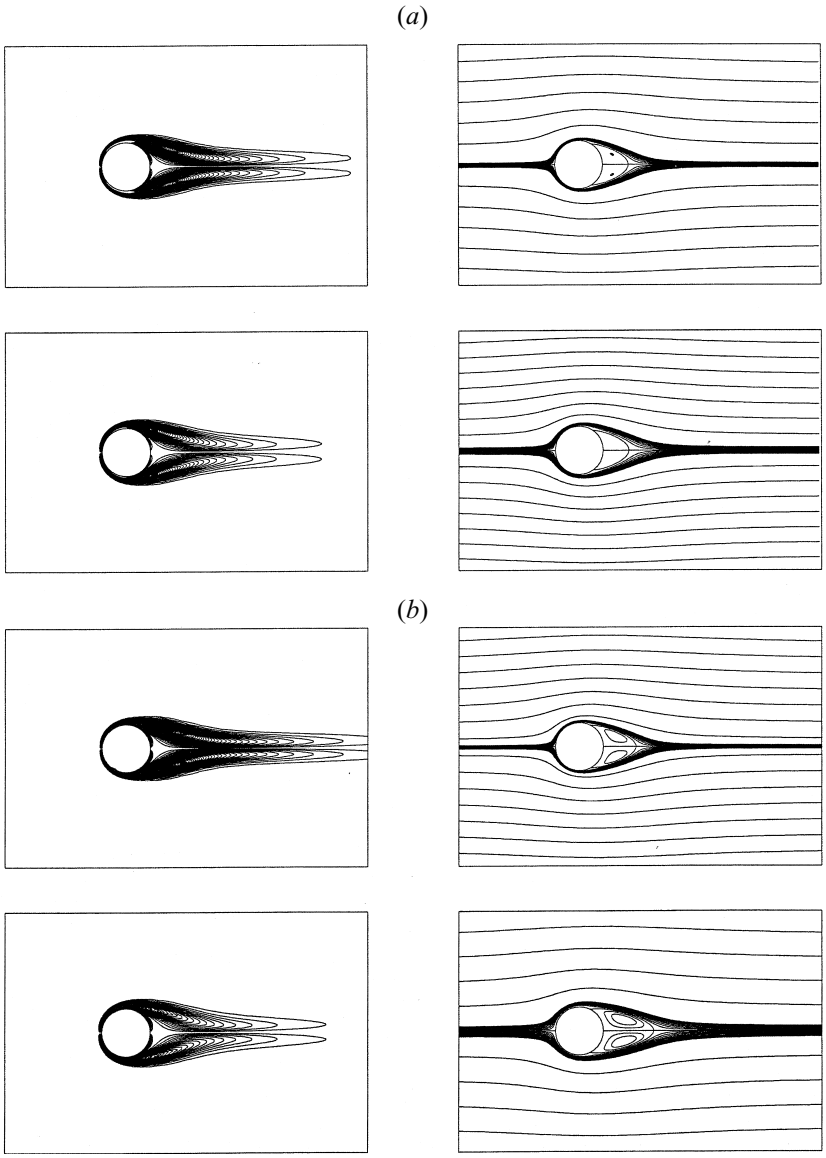


FIGURE 3 (*a–b*). For caption see facing page.

In figure 3(*c*) U_1 is increased to 1.8 and hence U_2 is reduced to 0.2. Again the vorticity contour plots show that the vorticity is advected slightly further downstream in the top layer compared to the bottom layer. Examining the vorticity in the lower layer it is noted that above (to the left of the cylinder looking downstream) the cylinder a contour of weak positive vorticity is observed and below (to the right of the cylinder looking downstream) the cylinder a contour of weak negative vorticity is seen, as well. This is similar to that observed in the one-layer β-plane retrograde flow modelled numerically by Page & Johnson (1990) and Matsuura & Yamagata (1986). This β-plane effect is seen due to the sloping of the interface between the two layers. It is not seen in the $\lambda = 0$ contour plots, because when $Ro = 0$ the slope of the interface is zero. In the one-layer β-plane experimental flows the β-effect is simulated by tilting

https://doi.org/10.1017/S0022112098002262 Published online by Cambridge University Press

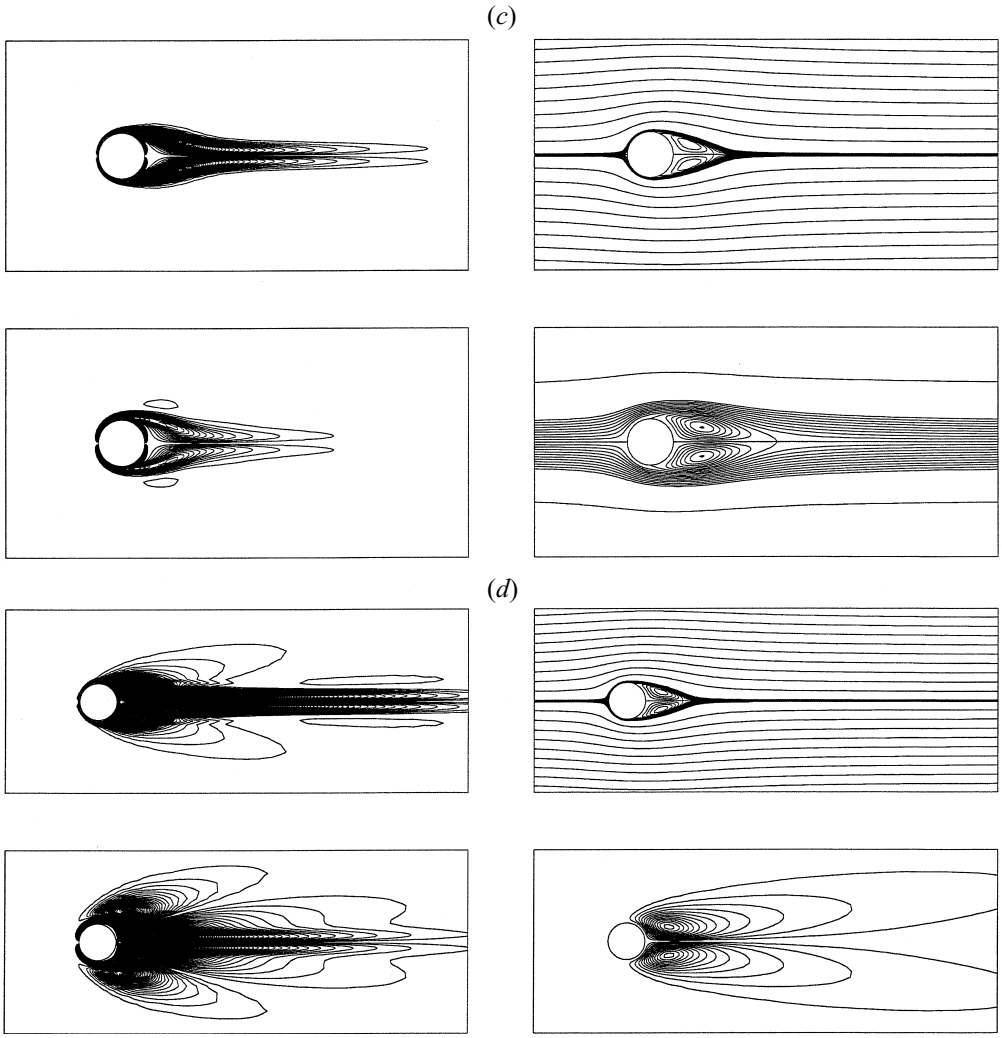


FIGURE 3. Contour plots of vorticity and streamfunction for $\lambda = 2$, $\delta = 0.1$, $F = 1$, $\chi = 1$ and (*a*) $U_1 = 1.2$, (*b*) $U_1 = 1.5$, (*c*) $U_1 = 1.8$ and (*d*) $U_1 = 2.0$. The contour interval is the same as figure 2 except that the contour interval of the vorticity is 0.01 when $U_1 = 2.0$.

the upper and lower surfaces of the channel (see, for example, Boyer & Davies 1982), thus the sloping of the interface in the two-layer flow produces similar effects. The contour plots of the streamfunction show that the length of the separated region in the upper layer is roughly the same size as the diameter as the cylinder, but that the separated region in the lower layer is much larger than that in the upper layer, being about two cylinder diameters long. The speed of the flow inside the separated region in the upper layer is quite slow. In contrast to this, the speed inside the separated region in the lower layer is of the same magnitude as for the flow just outside the shear layer.

For $U_1 = 2$ the speed in the lower layer vanishes at infinity and this flow is depicted in figure 3(*d*). The upper-layer contours of the vorticity extend a large distance downstream, compared to the weaker vertical shear cases, as would be expected. If very weak contours of vorticity are plotted a β-plane effect is observed (in figure 3(*d*) the vorticity contour interval is 0.01). Some distance downstream of

https://doi.org/10.1017/S0022112098002262 Published online by Cambridge University Press

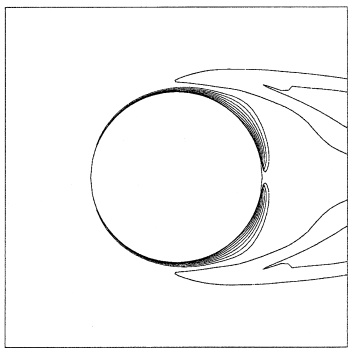


FIGURE 4. Contour plot of vorticity in the lower layer for $\lambda = 2$, $\delta = 0.1$ and $U_1 = 2.0$. The contour interval is 0.5.

the cylinder a weak contour of positive vorticity can be seen above the x-axis and a weak negative contour can be seen below the x-axis. Also, weak contours of vorticity can be seen extending away from the cylinder above and below the main contours of vorticity. Again, these features of the flow are similar to the one-layer prograde flows which have been modelled numerically by Page & Johnson (1990) and Matsuura & Yamagata (1986). This effect would also be seen in the weaker vertical shear cases if the smaller contours were plotted. An explanation of the β-effects in the one-layer flow are given in Blanchonette (1995). The contour plots of the streamfunction show that the bubble in the top layer is about one cylinder diameter in length. The width of the separated region has also increased and is greater than the diameter of the cylinder and the flow inside the bubble has become more rapid.

Studying the lower-layer vorticity contour plot it is noted that some of the vorticity is detached from the cylinder. This is because vorticity is not being generated directly by the boundary layer on the cylinder, but comes from the interaction between the two layers (a close up of the cylinder is shown in figure 4). In figure 3(d) contours of vorticity can also be seen above and below the cylinder; this is a result of the sloping interface discussed for the previous case. On the top surface of the cylinder positive vorticity is generated and negative vorticity is generated around the bottom of the cylinder. This is due to the flow being reversed right around the cylinder. Examining the contour plot of the streamfunction in the lower layer it can be seen that the separated region is massive and that most of the recirculation occurs on the downstream side of the cylinder, in contrast to the $\lambda = 0$ case. The horizontal extent of the 0.02 streamline is many times greater than the diameter of the cylinder. The spin up of the slower layer by the faster one causes the separated region in the slower layer to grow much larger and the recirculating flow to be more rapid than that in the upper layer. The coupling of the two layers causes the slower layer to behave in a way that could not be predicted from the one-layer flow.

As we have just seen the sloping of the interface between the two layers produces similar effects to those observed in the one-layer case with the top of the container being tilted to allow Rossby waves to propagate. The position of the interface between the two layers is proportional to $\psi_2 - \psi_1$. The contour plot of the interface height contours for the case just examined can be seen in figure 5. Away from the cylinder the slope is essentially linear and at the rear of the cylinder a small region can be seen where the interface is approximately level. Hence, flow features are observed that are quite similar to those observed in the prograde and retrograde cases.

https://doi.org/10.1017/S0022112098002262 Published online by Cambridge University Press

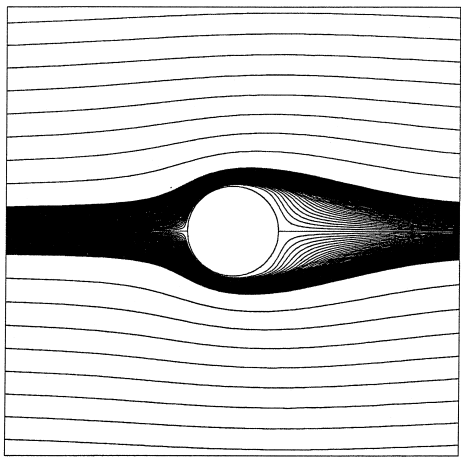


FIGURE 5. Contour plot of $\psi_2 - \psi_1$ for $\lambda = 2$, $\delta = 0.1$ and $U_1 = 2.0$. The contour interval is 1.0, except close to the cylinder where it is 0.02.

3.3. *The effect of increasing* δ

In the next series of contour plots, shown in figure 6, λ is kept constant at 2 (as in figure 3) and δ is increased to 0.2, so that the effect of strengthening the viscous diffusion can be examined. The same trends are noted as those observed in the one-layer flow. Briefly, the $E^{1/4}$ layer at the front of the cylinder has thickened and less vorticity is produced on the surface of the cylinder. Also, the separated regions are smaller and the recirculating flow is slower. However, when the vertical shear is strong the contour plot of the streamfunction is similar to that for the $\delta = 0.1$ case, although the recirculating flow is slower.

3.4. *Variation of bubble size with increasing vertical shear*

3.4.1. *The length of the separated region*

To gain more of an understanding about the change in the size of the separated regions with increasing vertical shear it is useful to plot the length of the separated region in both layers relative to the diameter of the cylinder as a function of the free-stream speed in the upper layer. The length of the separated region is defined as the distance from the rear of the cylinder to the point at which the zero streamlines, which enclose the recirculating region, meet. The length can also be defined in other ways, as there are difficulties associated with accurately identifying the zero streamline in the experiments, for example (see Matsuura & Yamagata 1985 or Page & Duck 1991).

A plot of the length of the separated region in both layers as a function of the vertical shear is shown in figure 7 for $\lambda = 2$ and $\delta = 0.1$. The length of the upper-layer separated region increases slowly and in a monotonic fashion as the vertical shear increases, similar to the trends noted in the one-layer case, since increasing the free-stream speed can be thought of as increasing the strength of the advective term in the vorticity equation. The size of the lower-layer separated region increases much more quickly and when $U_1 \approx 1.3$ the lower-layer separation bubble is longer than the upper-layer one. When $U_1 = 1.9$ the lower-layer bubble is nearly four diameters long, whilst the length of the separated region in the upper layer has yet to reach one cylinder diameter.

https://doi.org/10.1017/S0022112098002262 Published online by Cambridge University Press

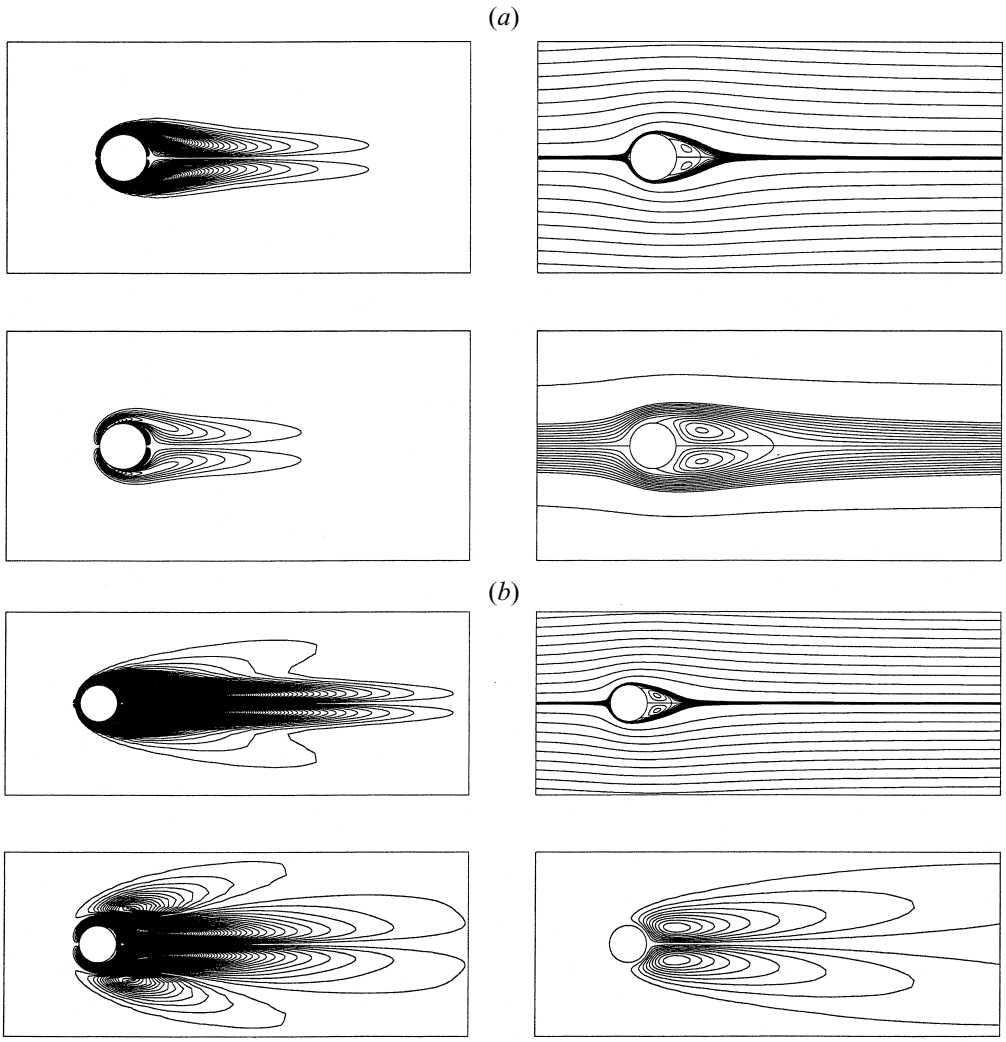


FIGURE 6. Contour plots of the vorticity and streamfunction for $\lambda = 2$, $\delta = 0.2$, $F = 1$, $\chi = 1$ and (*a*) $U_1 = 1.8$ and (*b*) $U_1 = 2.0$.

Similar trends to the one-layer case are noted when the strength of the viscous diffusion term is increased, the length of the separated regions being reduced, although when the vertical shear is strong the length of the separated region in the slower layer is approximately the same as the $\delta = 0.1$ case. On increasing the strength of the advection term similar trends are also noted to the one-layer flow.

3.4.2. *The width of the separated region*

In the one-layer case the width of the separation bubble changes little, if at all, except when the flow has just separated from the cylinder surface. In the two-layer case the width of the separated region in the upper layer behaves in a similar fashion to the one-layer flow; however in the lower layer the width of the bubble increases quickly as the vertical shear is increased. The width of the bubble (in this case) is defined as the maximum distance between the zero streamlines, which enclose the

https://doi.org/10.1017/S0022112098002262 Published online by Cambridge University Press

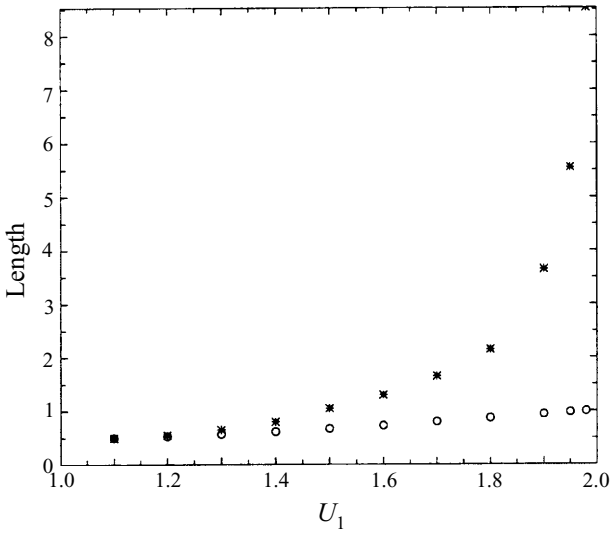


FIGURE 7. The length of the separated region as a function of increasing vertical shear in the upper (○) and lower (*) layers for $\lambda = 2$, $\delta = 0.1$.

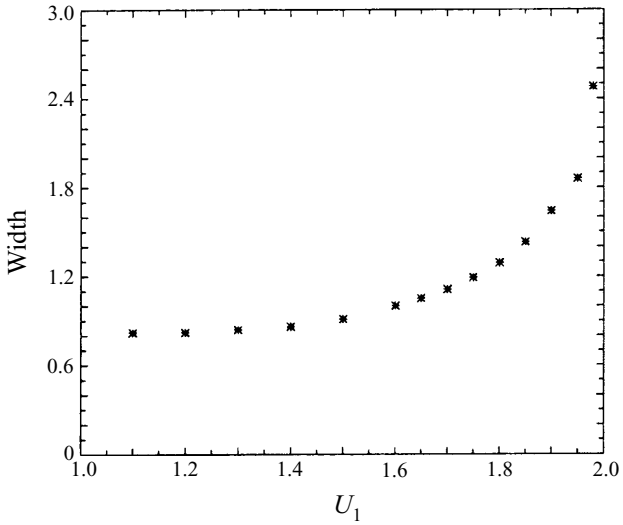


FIGURE 8. The width of the separated region in the lower layer with increasing vertical shear for $\lambda = 2$, $\delta = 0.1$.

separated region, relative to the diameter of the cylinder. The variation of the width of the upper-layer bubble will not be calculated since it changes only slightly in this layer.

In figure 8 the width of the separation bubble in the lower layer as a function of the vertical shear is plotted for $\lambda = 2$ and $\delta = 0.1$. Initially, when the vertical shear is weak, the growth of the width of the bubble increases slowly. As U_1 is increased to about 1.5 the width of the bubble begins to grow more rapidly and once $U_1 = 1.95$ it is about 1.85 cylinder diameters.

Increasing the strength of the viscous term produces the same trends noted in the one-layer case, although when the vertical shear is strong the width of the separated region is approximately the same as the $\delta = 0.1$ case. On increasing the strength of

https://doi.org/10.1017/S0022112098002262 Published online by Cambridge University Press

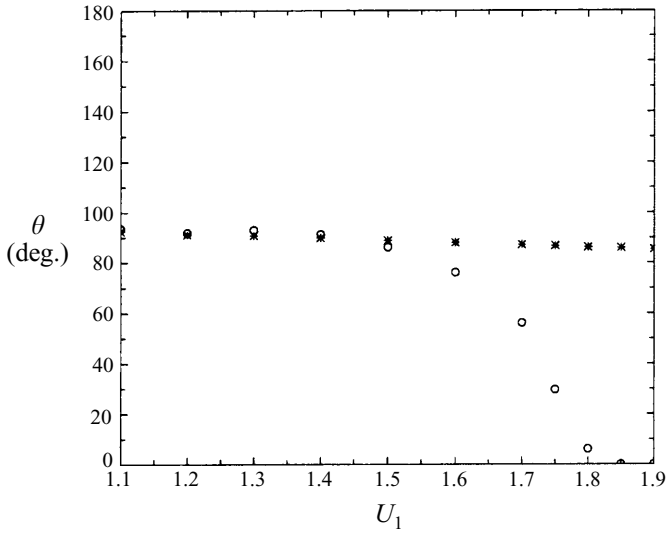


FIGURE 9. The variation of the separation point with increasing vertical shear using the adverse-pressure-gradient definition in the upper (*) and lower (○) layers for $\lambda = 2$, $\delta = 0.1$. θ is measured from the front stagnation point.

the advective term similar trends to the previous cases are noted. It must be noted at this point that the measurements of the length and width of the separated region become less accurate (compared to the weaker vertical-shear cases) as the size of the separation bubble increases since the grid becomes coarser further from the cylinder.

3.5. *Separation point*

One feature of the one-layer flow examined by Page (1987) was the variation of the separation point as λ was increased. It was found that, beyond the critical value for separation, the separation point moved from the rear stagnation point around towards 109° as λ was increased. That theory, however, was based on the properties of inviscid flows and it is not necessarily so obvious where the separation point is located in a viscous flow with a finite boundary-layer thickness. Batchelor (1967) reports that it is common for the point of zero shear stress to be taken as the point at which the flow separates. This is not strictly correct, as was pointed out by Brevdo & Merkine (1985), since it is possible to have reversed flow without the boundary layer actually separating from the cylinder. Another definition of separation is when $\partial p/\partial\theta = 0$ (Smith 1979); this is the point at which an adverse-pressure gradient develops on the surface of the cylinder. This point can also be expressed as when $\partial\zeta/\partial r = 0$. The issue of flow separation in this context is examined in more detail Blanchonette & Page (1997*b*). In the present study the point of separation was found using the adverse-pressure-gradient definition.

Figure 9 depicts the case $\lambda = 2$ and $\delta = 0.1$. When the vertical shear is weak the point of separation is very close in both layers at approximately 90° from the front stagnation point of the cylinder. As the vertical shear is increased the separation point of the upper layer moves quite slowly towards the front of the cylinder, in a similar fashion to the one-layer case. The flow separated at approximately 85°, measured from the front of the cylinder, when $U_1 = 1.9$. In contrast to this, when U_1 is increased beyond 1.6 the separation point in the lower layer moves quickly towards the front stagnation point.

https://doi.org/10.1017/S0022112098002262 Published online by Cambridge University Press

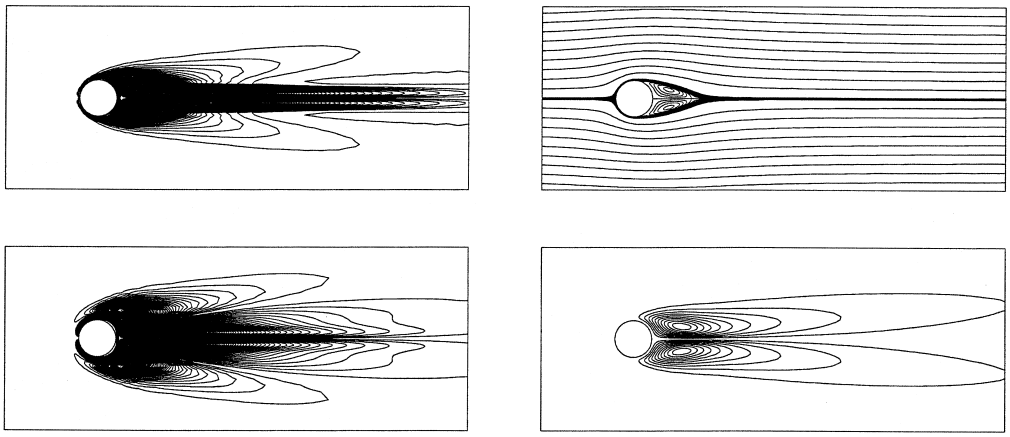


FIGURE 10. The contour plots of vorticity and streamfunction when $\lambda = 2$, $\delta = 0.1$ and $F = 2$ for $U_1 = 2.0$. The contour interval is the same as figure 3.

Increasing the strength of δ results in the flow in both layers separating closer to the rear of the cylinder, as is expected; however when the vertical shear is strong the flow in the slower layer separates at approximately the same point as in the $\delta = 0.1$ case. Increasing the strength of the advection term also produces similar trends to the one-layer case, the flow separating closer to the front stagnation point, although when the vertical shear is strong the flow in slower layer separates at about the same point as the $\delta = 0.1$ case.

3.6. *The effect of variation of the Froude number*

The flow in both layers can also be affected by the variation of the Froude number, which alters the slope of the interface. In this section the effect of reducing the Froude number to zero and increasing it to 2 will be examined.

In the following case the parameter values will be fixed at $\lambda = 2$, $\delta = 0.1$, $\chi = 1$ and $F = 2$. When the vertical shear is weak the flow in both layers is similar to that observed for the $F = 1$ case since the slope of the interface is small. As the strength of the shear is increased the effect of increasing the Froude number becomes clear. For the case $U_1 = 2.0$, shown in figure 10, the contours of the vorticity and streamfunction in the upper layer are essentially unchanged from the $F = 1$ case, except that the vorticity contours produced by the β-effect are stronger due to the increased slope of the interface, although they are still quite weak. This has also been shown in the corresponding one-layer prograde flow modelled numerically by Matsuura & Yamagata (1986). In the lower layer the vorticity contours are advected slightly further downstream and the β-plane effect has been intensified compared to the $F = 1$ case. The streamfunction contour plot shows that the width of the recirculation region has decreased and the length has increased. This is was also found by Matsuura & Yamagata (1986) for their numerically modelled one-layer retrograde flows. As they explain this is caused by the long Rossby waves enhancing the advection of vorticity.

The length of the separated region in the upper and lower layers shows very little difference to the $F = 1$ case, shown in figure 7, although when the vertical shear is strong the bubble in the lower layer is narrower and longer than for the $F = 1$ case,

https://doi.org/10.1017/S0022112098002262 Published online by Cambridge University Press

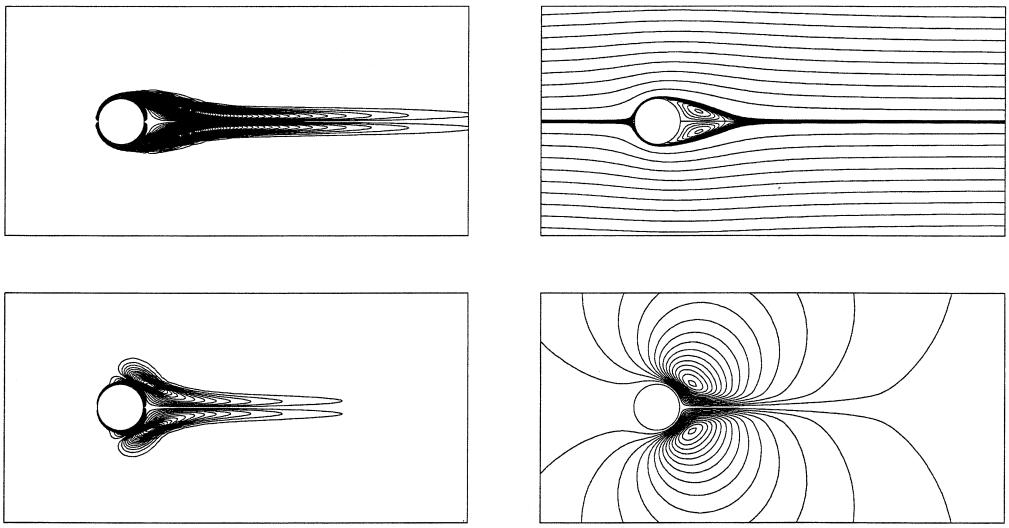


FIGURE 11. The contour plots of the vorticity and streamfunction for $\lambda = 2$, $\delta = 0.1$, $F = 0$ with $U_1 = 2.0$. In this case the vorticity contour interval is 0.1 for all the plots.

due to the increased β-plane effect discussed previously. Furthermore, increasing the Froude number has little effect on the position of separation.

Next, we will consider the case where the Froude number is reduced to zero and in this case the interface remains level. The contour plots of the streamfunction and vorticity for the same parameter values as the previous case, but with $F = 0$ are shown in figure 11. When the vertical shear is weak the effect of reducing the Froude number to zero is small. This is to be expected since when the vertical shear is weak the slope of the interface is small (for non-zero Froude numbers), hence the β-effect is small.

On increasing U_1 to 1.8 no significant difference can be seen in the upper-layer contours of the vorticity and streamfunction. However, in the lower layer the effect of reducing the Froude number can be clearly seen. The contours of the vorticity are not advected as far downstream and the contour plot of the streamfunction shows that the bubble is shorter and wider and the recirculating flow is more rapid compared to the $F = 1$ case, shown in figure 3. Since the interface is flat long Rossby waves can no longer be generated in the lower layer, thus the bubble is shorter and wider than for the non-zero Froude number cases.

When $U_1 = 2$ (figure 11) the contour plots of the streamfunction and vorticity in the upper layer show similar trends to the $U_1 = 1.8$ case. Since the slope of the interface is zero the β-plane effect noted in the previous cases is not observed in either layer. Turning our attention to the lower layer, the vorticity contours produced by the spin up of the slower layer by the faster one do not extend as far downstream as the $F = 1$ case and they appear more rounded at the point closest to the cylinder. The separation bubble is shorter and much wider than when $F = 1$; the bubble also extends upstream past the cylinder since the strength of the adverse-pressure gradient has increased. Compared to the $F = 1$ case the spin up of the lower layer by the upper one has increased, since the interface remains level (hence the vertical velocity at the edge of the Ekman layer has increased compared to the $F = 1$ case).

https://doi.org/10.1017/S0022112098002262 Published online by Cambridge University Press

Graphs of the separation point of the flow as a function of the vertical shear show very little variation from the $F = 1$ case, illustrated in figure 9 although when the vertical shear is strong the flow separates closer to the front of the cylinder in the lower layer compared to the $F = 1$ case. This is to be expected, since reducing the Froude number to zero increases the spin up of the slower layer by the faster one, hence the adverse-pressure gradient on the cylinder increases.

The size of the separated region in the upper layer is not affected significantly by reducing the Froude number. When the vertical shear is small the length and width of the bubble in the lower layer varies little from that when $F = 1$. However, as the vertical shear is increased the bubble in the lower layer is wider and shorter than the $F = 1$ case, which is to be expected since long Rossby waves can no longer propagate downstream.

4. Discussion

The flow past a cylinder in a rotating frame is a basic problem in geophysical fluid dynamics. The two-layer problem allows the effect of stratification to be considered in the simplest way possible. In this paper the problem has been modelled numerically, the main focus being to examine in detail the effect of variation of the vertical shear while keeping the other parameters the same in both layers. The calculations revealed some quite surprising results that could not be predicted from the one-layer flows.

The contour plots of the streamfunction and the vorticity showed that the flow in the faster layer displayed similar trends to those noted in the one-layer flows. In the slower layer the flow also behaved in a similar fashion to the one-layer flow when the vertical shear was weak. However, when the strength of the vertical shear increased the flow in this layer behaved in a fashion that could not be predicted from the one-layer flow, with the size of the separated region growing quickly. This rapid increase in the size of the separated region is due to the spin up of this layer by the faster one. Since the interface between the two layers could slope, a weak β-plane effect was observed in both layers of fluid that resembled the β-effects observed in the one-layer flow. In the faster layer this effect was found to be similar to the prograde flows, while in the lower one it resembled the retrograde flows.

To further our understanding of the effect of varying the vertical shear the size of the separated region in both layers was measured as a function of the vertical shear. The length of the separated region in the faster layer increased monotonically in a similar fashion to that observed in the one-layer flow. However, in the slower layer the length and width of the separated region grew rapidly as the vertical shear increased. Increasing the Froude number (and hence the slope of the interface) was found to increase the length and decrease the width of the separated region in the slower layer, although it did not have a significant effect on the separated region in the faster layer. The variation of the separation point was also investigated and again the faster layer showed similar trends to the one-layer case, the separation point moving slowly towards the front stagnation point. However, as the vertical shear was increased the separation point in the slower layer moved quickly towards the front of the cylinder. Interestingly, when the vertical shear was strong the size of the separated region and separation point of the flow in the slower layer did not change significantly when the strength of the viscous diffusion was increased.

The two-layer boundary-layer flow past a cylinder on a f-plane has also been investigated theoretically by Brevdo & Merkine (1985). The results of the present study will be compared and contrasted to that study in Blanchonette & Page (1998).

https://doi.org/10.1017/S0022112098002262 Published online by Cambridge University Press

I wish to thank Michael Page for his assistance with this paper. I would also like to thank the three referees for their helpful suggestions.

REFERENCES

Baines, P. G. 1979 Observations of stratified flow past three-dimensional obstacles. *J. Geophys. Res.* **84**, 7834–7838.

Batchelor, G. K. 1967 *An Introduction to Fluid Dynamics*. Cambridge University Press.

Becker, A. 1989 Flow separation in a rotating fluid. PhD Thesis Monash University.

Blanchonette, P. 1995 The flow past a cylinder in a rotating frame. PhD Thesis Monash University.

Blanchonette, P. 1997 The flow past a cylinder in a rotating frame. Submitted to *J. Fluid Mech.*

Blanchonette, P. & Page, M. A. 1997 Boundary-layer separation in the two-layer flow past a cylinder in a rotating frame. Submitted to *Theor. Comput. Fluid Dyn.* **11**, 95–108.

Boyer, D. L. & Davies, P. A. 1982 Flow past a circular cylinder on a β-plane. *Phil. Trans. R. Soc. Lond.* A **306**, 533–556.

Brevdo, L. & Merkine, L. 1985 Boundary-layer separation of a two-layer rotating flow on a f-plane. *Proc. R. Soc. Lond.* A **400**, 75–95.

Etling, D. 1990 Mesoscale vortex shedding from large islands: a comparison with laboratory experiments of rotating stratified flows. *Met. Atmos. Phys.* **43**, 145–151.

Greenspan, H. P. 1968 *The Theory of Rotating Fluids*. Cambridge University Press.

Israeli, M. 1972 On the evaluation of iteration parameters for the boundary vorticity. *Stud. Appl. Maths* **51**, 67–71.

Matsuura, T. & Yamagata, T. 1985 A numerical study of viscous flow past a right circular cylinder on a f-plane. *J. Met. Soc. Japan* **63**, 151–166.

Matsuura, T. & Yamagata. T. 1986 A numerical study of viscous flow past a right circular cylinder on a β-plane. *Geophys. Astrophys. Fluid Dyn.* **37**, 129–164.

Merkine, L. & Brevdo, L. 1986 Boundary-layer separation of a two-layer rotating flow on a β-plane. *J. Fluid. Mech.* **167**, 31–48.

Page, M. A. 1987 Separation and free-streamline flows in a rotating fluid at low Rossby numbers. *J. Fluid Mech.* **194**, 493–500.

Page, M. A. & Duck, D. W. 1991 The structure of separated flow past a circular cylinder in a rotating frame. *Geophys. Astrophys. Fluid Dyn.* **58**, 197–223.

Page, M. A. & Johnson, E. R. 1990 Flow past cylinderical obstacles on a beta-plane. *J. Fluid Mech.* **221**, 349–382.

Smith, F. T. 1979 Laminar flow of an incompressible fluid past a bluff body: the separation, reattachment, eddy properties and drag. *J. Fluid Mech.* **92**, 171–205.

Thompson, L. 1993 Two-layer quasi-geostrophic flow over finite isolated topography. *J. Phys. Oceanogr.* **23**, 1297–1314.

Zeeuw, P. M. de 1990 Matrix-dependent prolongation and restrictions in a blackbox multi-grid solver. *J. Comput. Appl. Maths* **33**, 1–27.

https://doi.org/10.1017/S0022112098002262 Published online by Cambridge University Press